Structure Research of Resistance Shunt Type Piezoelectric Composite and Underwater Sound Absorption Performance Analysis

Yang Sun

College of Science, Beijing Forestry University, No.35 Tsinghua East Road, Haidian District, Beijing, China, 100083. E-mail: sunyang@bjfu.edu.cn

Bo Hua

Systems Engineering Research Institute, China State Shipbuilding Corporation, No.1 Fengxian East Road, Haidian District, Beijing, China, 100094.

(Received 30 May 2023; accepted 3 September 2023)

The high-efficiency sound absorption of underwater sound-absorbing materials under "low frequency" and "wide frequency" conditions has become a hot topic in current research. Underwater semi-active sound absorption can help to improve low frequency sound absorption performance by designing the structure of the piezoelectric composite and the shunt circuits, and it is also advantageous due to its simplicity, compactness, ease of installation, low cost, and high stability. In this paper, a kind of resistance shunt type piezoelectric composite is designed, and its underwater sound absorption performance is analyzed. Theoretical analytical formulas and finite element numerical calculation are used to calculate the electro-elastic constants of the piezoelectric composite. The theoretical model based on the Mason equivalent circuit and transfer matrix theory is used to calculate the sound absorption coefficient. Through the study of 0-3 and 1-3 composites used in the existing research work, it was found that the piezoelectric composite which is suitable for resistance shunt type underwater semi-active sound absorption should have a low longitudinal wave velocity and high electromechanical conversion coefficient. According to this design objective, the structure of the piezoelectric composite has been gradually modified, and finally it is determined that the sparse oblique 2-1-3 composite is an appropriate type of piezoelectric composite. Theoretical calculations and simulation experimental measurement verifies that when the inclination angle is 21° and the shunt resistance is 10 kΩ or the inclination angle is 24° and the shunt resistance is 10 kΩ, the sound absorption coefficient within the low frequency band 1–3 kHz can be significantly improved.

NOMENCLATURE

ω	angular frequency
k	wave number
ρ	density
c	longitudinal wave velocity
l	thickness
S	cross-sectional area
C_0	inherent capacitance
n	electromechanical conversion coefficient
R_x	shunt resistance
A	sound absorption coefficient
θ	inclination angle of oblique composites
ϕ	volume fraction of piezoelectric phase in 0-3 composite
μ	volume fraction of piezoelectric phase in 1-3 and 2-1-3 composites
A	aspect ratio
β	ratio of thickness of piezoelectric layer and thickness of 2-1-3 composite

1. INTRODUCTION

One important application of underwater sound-absorbing materials is to absorb the sound waves emitted by active sonar and reduce the acoustic target intensity of the underwater vehicles. Underwater sound-absorbing materials usually require limited thickness, matching acoustic impedance with water, high loss factor, and high compressive strength.[1] The sound absorption frequency range of underwater sound-absorbing materials is determined by the operating frequency range of the active sonar system. With the development of low-frequency sonar, the high-efficiency sound absorption of underwater sound-absorbing materials under "low frequency" and "wide frequency" conditions has become a hot topic in current research.[2]

Underwater sound absorption is mainly comprised of passive sound absorption, active sound absorption, and semi-active sound absorption. Passive sound absorption uses viscoelastic materials with a cavity structure,[3–5] rigid inclusions, or scatterers[6] as the sound-absorbing material and reduces or eliminates the reflection of incident sound waves through energy attenuation. The sound absorption performance of passive sound absorption is good within the middle and high fre-

quency band but is limited within the low frequency band. Active sound absorptio[7,8] first analyzes changes in sound source characteristics, then controls and adjusts the surface acoustic impedance of the sound-absorbing material to match the acoustic impedance of water, so that the incident sound wave can pass through the interface without reflection. The sound absorption performance of active sound absorption is good within the low frequency band, however, the signal processing process is complex, and there are a few unstable factors. There are large delays in processing high-frequency acoustic signals, and there is a risk of self-exposure due to active sound radiation. Semi-active sound absorption[9–14] uses piezoelectric composites with good flexibility and low acoustic impedance as the sound-absorbing material. Since the matrix of the piezoelectric composite is made of viscoelastic material, the sound energy attenuation of passive sound absorption still applies. Additionally, the sound-absorbing material is connected with the shunt circuit, and therefore the piezoelectric shunt damping sound-absorbing mechanism is added. Semi-active sound absorption can help to improve the low frequency sound absorption performance by designing the structure of the piezoelectric composite and the shunt circuits. It also has the advantages of simplicity, compactness, ease of installation, low cost, and high stability.

Piezoelectric shunt damping technology[15,16] has been widely used in the fields of structural vibration control,[17] sound absorption.[18] and sound insulation in the air.[19,20] However, in the field of underwater sound absorption, this technology has not been as widely applied or researched. Some relevant studies are summarized below. Zhang et al.[9] established an electro-acoustic model of a single piezoelectric layer covering a rigid boundary and theorized about the influence of different shunt circuits and different piezoelectric materials on sound absorption performance. Yu et al.[10] established a one-dimensional model of 0-3 piezoelectric composite sound-absorbing coating and improved the sound absorption coefficient within the wide band range of 1–7 kHz by introducing resistor and negative capacitor series shunt circuits. Feng et al.[11] designed a new type of piezoelectric shunt damping sound-absorbing layer made of 0-3 composite, PZT and rubber and successfully improved the low frequency absorption coefficient. Sun et al.[12] proposed an underwater sound-absorbing coating composed of multiple 1-3 composite layers and designed the shunt impedance of each layer when the sound absorption coefficients at specific frequencies are restricted. Zhang et al.[13] designed an underwater semi-active composite sound-absorbing coating with periodic subwavelength piezoelectric arrays and studied the influence of seven critical parameters on the sound absorption characteristics. Wang et al.[14] studied tunable underwater low-frequency sound absorption of the locally resonant piezoelectric metamaterials (LRPM) and significantly improved the sound absorption bandwidth by introducing negative capacitance.

The above studies about underwater semi-active sound absorption still have some problems in the implementation of shunt circuits, sound absorption frequency range, and compressive strength. Authors of some publications[9–11,14] all proposed that the shunt circuit should contain negative capacitance, and Sun et al.[12] proposed that the shunt circuit should contain negative resistance. The realization of negative capacitance and negative resistance requires active components such as operational amplifiers and requires high stability and accuracy. Although Sun et al.[12] give the shunt impedance under the condition of restricting the sound absorption coefficients at specific frequencies, only the sound absorption coefficient within the middle frequency band 5–20 kHz can be controlled, while the sound absorption coefficient within the low frequency band 0–3 kHz has not been effectively improved. Zhang et al.[13] proposed composite anechoic coating consists of five different layers, and two of them contain a cavity structure. The cavity structure will deform under a certain hydrostatic pressure load. Consequently, the overall thickness of the anechoic coating will become thinner, and the stability will decrease.

In order to solve these problems, in this paper, a kind of resistance shunt type piezoelectric composite is designed, and its underwater sound absorption performance is predicted. The sound-absorbing coating is composed of a piezoelectric composite layer connected with shunt resistance. This structure is relatively simple, and the compressive strength is good. The sound absorption coefficient within the low frequency band 1–3 kHz can be effectively improved. The sound absorption coefficient is calculated using an established theoretical model based on the Mason equivalent circuit and transfer matrix theory and is measured in a finite element simulation experiment based on the pipe pulse method. The electro-elastic constants of piezoelectric composites are calculated by theoretical analytical formulas (0-3 type, dense 1-3 type and dense oblique 1-3 type) and the finite element numerical calculation (a sparse 1-3 type, a sparse oblique 1-3 type and a sparse oblique 2-1-3 type). The design idea of the piezoelectric composite structure is as follows. Through the study of 0-3 and 1-3 composites used in the existing research work, the physical properties of the piezoelectric composite that is suitable for resistance shunt type underwater semi-active sound absorption are explored first. Then, according to the design objective of the physical properties, the structure of the piezoelectric composite is gradually modified until it meets the prospective sound absorption performance.

2. THEORETICAL MODEL

2.1. Theoretical Model of Sound Absorption Coefficient Calculation

A one-dimensional electro-acoustic model is established to calculate the semi-active sound absorption coefficient of the piezoelectric composite coating, and a schematic diagram of sound wave propagation is shown in Fig. 1(a). The piezoelectric composite coating is adhered to a steel backing, and the contact surface is called Interface 2. The piezoelectric composite coating is adjacent to water, and the contact surface is Interface 1. The steel backing is adjacent to air, and the contact surface is Interface 3. It is assumed that the transverse dimensions of the piezoelectric composite coating and the steel backing are much larger than their respective thicknesses, and they only compress in their thickness direction. Therefore, there

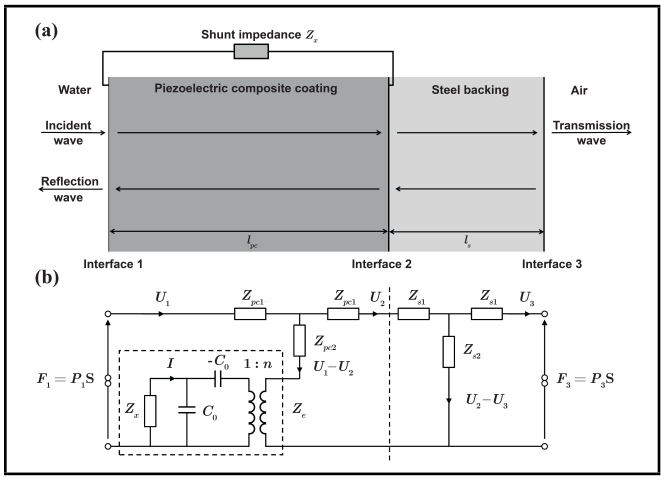

Figure 1. Theoretical model of sound absorption coefficient calculation. (a) schematic diagram of sound wave propagation; (b) electromechanical equivalent circuit.

are only longitudinal waves within each medium. Water and air are assumed to be semi-infinite. The piezoelectric composite coating is connected to a shunt circuit, and the shunt impedance is Z_x. A plane sound wave from the water penetrates the piezoelectric composite coating and the steel backing perpendicularly and then enters the air. The sound wave will reflect and transmit on the three interfaces. Due to the positive piezoelectric effect of the piezoelectric composite, the mechanical energy of the sound wave will be converted into electrical energy. Then the electrical energy can be dissipated in the form of heat through the shunt circuit. This is the mechanism of underwater semi-active sound absorption.

The electromechanical equivalent circuits of the piezoelectric composite and the steel backing can be obtained using mechanical vibration equations. Since the piezoelectric composite adheres to the steel backing, the electromechanical equivalent circuits of the two parts are in parallel, as shown in Fig. 1(b).

Where F_1 and F_3 are the forces applied on Interface 1 and 3. P_1 and P_3 are the sound pressures. U_1, U_2 and U_3 are the particle velocities on the respective Interface 1, 2 and 3. $Z_{pc1} = j\rho_{pc}c_{pc}Stan(k_{pc}l_{pc}/2)$ and $Z_{pc2} = \rho_{pc}c_{pc}S/\left[jsin(k_{pc}l_{pc})\right]$ are the mechanical impedances of the piezoelectric composite. The subscript pc represents the piezoelectric composite. $k_{pc} = \omega/c_{pc}, \rho_{pc}, c_{pc}, l_{pc}$, and S are the wavenumber, the density, the longitudinal wave velocity, the thickness and the cross-sectional area of the piezoelectric composite, respectively. $C_0 = \epsilon^S_{33pc}S/l_{pc}$ is the inherent capacitance and $n = e_{33pc}S/l_{pc}$ is the electromechanical conversion coefficient. e^S_{33pc} is the dielectric constant component and e_{33pc} is the piezoelectric constant component. Z_x is the shunt impedance and $Z_\epsilon = n^2\left[Z_x/(1+j\omega_0C_0Z_x) - 1/(j\omega_0C_0)\right]$ is the impedance within the dashed box. $Z_{s1} = j\rho_s c_s Stan(k_s l_s/2)$ and $Z_{s2} - \rho_s C_s S/[jsin(k_s l_s)]$ are the mechanical impedances of the steel backing. The subscript s represents the steel backing. $k_s = \omega/c_s$, ρ_s, c_s and l_s are the wavenumber, the density, the longitudinal wave velocity and the thickness of the steel backing, respectively. The cross-sectional area of the steel backing is the same as that of the piezoelectric composite coating.

According to the equivalent circuit, the relationship between the pressures P_1, P_3 and the particle velocities U_1, U_3 can be obtained as follows:

$$\begin{pmatrix} P_1 \\ U_1 \end{pmatrix} = B_p B_s \begin{pmatrix} P_3 \\ U_3 \end{pmatrix} = B \begin{pmatrix} P_3 \\ U_3 \end{pmatrix}; \tag{1}$$

where B_p is the transfer matrix of the pressures and particle velocities on Interfaces 1 and 2:

$$B_p = \begin{pmatrix} \frac{x_1}{x_2} & \frac{x_1^2 - x_2^2}{x_2} \\ \frac{1}{x_2} & \frac{x_1}{x_2} \end{pmatrix}; \tag{2}$$

$$x_1 = \frac{Z_{pc1} + Z_{pc2} + Z_e}{S}; \tag{3}$$

$$x_2 = \frac{Z_{pc2} + Z_e}{S}. \tag{4}$$

B_s is the transfer matrix of the pressures and particle velocities on Interfaces 2 and 3:

$$B_s = \begin{pmatrix} \cos(k_s l_s) & j\rho_s c_s \sin(k_s l_s) \\ \frac{j\sin(k_s l_s)}{\rho_s c_s} & \cos(k_s l_s) \end{pmatrix}. \tag{5}$$

B is the transfer matrix of the pressures and particle velocities on Interfaces 1 and 3, which can be written as:

$$B = B_p B_s = \begin{pmatrix} b_{11} & b_{12} \\ b_{21} & b_{22} \end{pmatrix}. \tag{6}$$

The surface acoustic impedance on Interface 1 is the quotient of the pressure P_1 and the particle velocity U_1:

$$Z_{1i} = \frac{P_1}{U_1} = \frac{b_{11}P_3 + b_{12}U_3}{b_{21}P_3 + b_{22}U_3} = \frac{(P_3/U_3)b_{11} + b_{12}}{(P_3/U_3)b_{21} + b_{22}} = \frac{\rho_a c_a b_{11} + b_{12}}{\rho_a c_a b_{21} + b_{22}}; \tag{7}$$

where $P_3/U_s = \rho_a c_a$ is the acoustic impedance of air.

Because the acoustic impedance of semi-infinite air is far less than that of the steel backing, an approximate-total reflection will occur on Interface 3. Hence it is reasonable to assume that the sound transmission coefficient is zero and, therefore, the sound absorptio coefficient is the difference between 1 and the sound reflection coefficient R,

$$A = 1 - R = 1 - \left|\frac{P_{1r}}{P_{1i}}\right|^2 = 1 - \left|\frac{Z_{1i} - \rho_w c_w}{Z_{1i} + \rho_w c_w}\right|^2; \tag{8}$$

where $P_1 i$ and $P_1 r$ are the amplitudes of the incident and reflection sound pressures on Interface 1, respectively. ρ_w and c_W are the density and the longitudinal wave velocity of water, and $\rho_w c_w$ is the acoustic impedance of water.

2.2. Theoretical Model of 0-3 Piezoelectric Composite

At present, the piezoelectric composites used in underwater semi-active sound absorption research include 0-3 composite[10] and 1-3 composite.[12] The 0-3 composite is composed of the matrix phase and the piezoelectric particles dispersed in the matrix phase. The matrix phase is generally made of polymer, such as rubber, and the piezoelectric phase is generally

made of piezoelectric ceramic. According to the theoretical model of 0-3 composite established by Furukawa,[21] its elastic constant component $c^D_{33(0-3)}$ dielectric constant component $\epsilon^S_{33(0-3)}$ and piezoelectric constant component $h_{33(0-3)}$ are respectively:

$$c^D_{33(0-3)} = \frac{2+3\phi}{2(1-\phi)} c_{33m} c^D_{33(0-3)} = \frac{2+3\phi}{2(1-\phi)} c_{33m}; \quad (9)$$

$$\epsilon^S_{33(0-3)} = \frac{1+2\phi}{1-\phi} \epsilon_m \epsilon^S_{33(0-3)} = \frac{1+2\phi}{1-\phi} \epsilon_m; \quad (10)$$

$$h_{33(0-3)} = \frac{15\phi}{2(1+2\phi)(1-\phi)} \cdot \frac{c_{33m}}{c^D_{33p}} h_{33p}; \quad (11)$$

where ϕ is the volume fraction of the piezoelectric phase in the 0-3 composite. The subscript m represents the matrix phase, p represents the piezoelectric phase, and (0-3) represents the 0-3 composite. c_{33m} and ϵ_m are the elastic constant component and dielectric constant component of the matrix phase, respectively. c^D_{33p} and h_{33p} are the elastic constant component and the piezoelectric constant component of the piezoelectric phase, respectively.

The density of 0-3 composite is:

$$\rho_{(0-3)} = \rho_m(1-\phi) + \rho_p \phi; \quad (12)$$

where ρ_m andρ_p are the densities of the matrix phase and the piezoelectric phase, respectively. The longitudinal wave velocity and electromechanical conversion factor of the 0-3 composite are:

$$c_{(0-3)} = \sqrt{\frac{c^D_{33(0-3)}}{\rho_{(0-3)}}}; \quad (13)$$

$$n_{(0-3)} = \frac{h_{33(0-3)} \epsilon^S_{33(0-3)} S}{l_{(0-3)}}. \quad (14)$$

2.3. Theoretical Model of a Dense 1-3 Piezoelectric Composite

The 1-3 composite is composed of the matrix phase and the piezoelectric rods vertically embedded in the matrix phase. According to the theoretical model of a dense 1-3 composite established by W.A. Smith,[22] its elastic constant components $c_{33}(1-3)^E$ and $c_{33}(1-3)^D$, dielectric constant component $\epsilon_{33}(1-3)^S$ and piezoelectric constant component $e_{33(1-3)}$ are respectively:

$$c^E_{33(1-3)} = \mu \left[c^E_{33p} - \frac{2(1-\mu)(c^E_{13p} - c_{12m})^2}{\mu(c_{11m}+c_{12m}) + (1-\mu)(c^E_{11p}+c^E_{12p})} \right] + (1-\mu) c_{11m}; \quad (15)$$

$$c^D_{33(1-3)} = c^E_{33(1-3)} + \frac{e^2_{33(1-3)}}{\epsilon^S_{33(1-3)}}; \quad (16)$$

$$\epsilon^S_{33(1-3)} = \mu \left[\epsilon^S_{33p} + \frac{2(1-\mu) e^2_{31p}}{\mu(c_{11m}+c_{12m}) + (1-\mu)(c^E_{11p}+c^E_{12p})} \right] + (1-\mu)\epsilon_m; \quad (17)$$

$$e_{33(1-3)} = 24\mu \left[e_{33p} - \frac{2(1-\mu) e_{31p}(c^E_{13p} - c_{12m})}{\mu(c_{11m}+c_{12m}) + (1-\mu)(c^E_{11p}+c^E_{12p})} \right]; \quad (18)$$

where μ is the volume fraction of the piezoelectric phase in the 1-3 composite, and the subscript (1-3) represents the 1-3 composite. The parameters of the matrix phase include the elastic constant components c_{11m} and c_{12m} , and the dielectric constant component ϵ_m. The parameters of the piezoelectric phase include the elastic constant components c^E_{11p}, c^E_{12p}, c^E_{13p} and c^E_{33p}, the dielectric constant component ϵ^S_{33p} and the piezoelectric constant components e_{31p} and e_{33p}.

The density, longitudinal wave velocity and electromechanical conversion factor of the 1-3 composite are respectively:

$$\rho_{(1-3)} = \rho_m(1-\mu) + \rho_p \mu; \quad (19)$$

$$c_{(1-3)} = \sqrt{\frac{c^D_{33(1-3)}}{\rho_{(1-3)}}}; \quad (20)$$

$$n_{(1-3)} = \frac{e_{33(1-3)} S}{l_{(1-3)}}. \quad (21)$$

2.4. Theoretical Model of a Dense Oblique 1-3 Piezoelectric Composite

If the piezoelectric rods of the 1-3 composite are embedded in the matrix phase obliquely and the inclination angle is θ, the property of the composite will have more changes. This material was first proposed by A. Baz et al.[23] and was called active piezoelectric damping composite (APDC). In this paper, it is referred to as an oblique 1-3 piezoelectric composite.

When the composite is of fine lateral spatial scale, it is called a dense oblique 1-3 composite. In this condition, the vertical strains are the same in both the piezoelectric phase and matrix phase, and so are the shear strains.

$$S^p_z = S^m_z = S_z; \quad (22)$$

$$S^p_{yz} = S^m_{yz} = S_{yz}. \quad (23)$$

According to the theoretical model of a dense oblique 1-3 composite established by A. Baz,[23] its elastic constant components $c^E_{33(obl1-3)}$ and $c^D_{33(obl1-3)}$, dielectric constant component $\epsilon^S_{33(obl1-3)}$ and piezoelectric constant component $e_{33(obl1-3)}$ are respectively:

$$c^E_{33(obl1-3)} = (1-\mu)M(c^m_{12} - c^p_{31}) + (1-\mu)X(c^m_{12} - c^p_{32}) + (1-\mu)c^m_{11} + \mu c^p_{33}; \quad (24)$$

$$c^D_{33(obl1-3)} = c^E_{33(obl1-3)} + \frac{e^2_{33(obl1-3)}}{\epsilon^S_{33(obl1-3)}}; \quad (25)$$

$$\epsilon^S_{33(obl1-3)} = (\mu-1)Oc^p_{91} + (\mu-1)Zc^p_{92} + \mu c^p_{99} + (1-\mu)\epsilon^m_x; \quad (26)$$

$$e_{33(obl1-3)} = -[(1-\mu)O(c_{12}^m - c_{31}^p) + (1-\mu)Z(c_{12}^m - c_{32}^p) + \mu c_{39}^p]; \quad (27)$$

where μ is the volume fraction of the piezoelectric phase and the subscript $(obl1-3)$ represents the dense oblique 1-3 composite. The c_{11}^m, c_{12}^m and ϵ_x^m are the elastic constant components and dielectric constant component of the matrix phase. The c_{31}^p, c_{32}^p, c_{33}^p, c_{39}^p, c_{91}^p, c_{92}^p, and c_{99}^p are the electro-elastic constant components of the piezoelectric phase. X, Z, M, O are the middle parameters and are expressed as:

$$X = \frac{(c_{13}^p - c_{12}^m)(c_{12}^m + fc_{21}^p) - (c_{23}^p - c_{12}^m)(c_{11}^m + fc_{11}^p)}{(c_{12}^m + fc_{12}^p)(c_{12}^m + fc_{21}^p) - (c_{11}^m + fc_{22}^p)(c_{11}^m + fc_{11}^p)}; \quad (28)$$

$$Z = \frac{c_{19}^p(c_{12}^m + fc_{21}^p) - c_{29}^p(c_{11}^m + fc_{11}^p)}{(c_{12}^m + fc_{12}^p)(c_{12}^m + fc_{21}^p) - (c_{11}^m + fc_{22}^p)(c_{11}^m + fc_{11}^p)}; \quad (29)$$

$$M = \frac{(c_{13}^p - c_{12}^m)(c_{11}^m + fc_{22}^p) - (c_{23}^p - c_{12}^m)(c_{12}^m + fc_{12}^p)}{(c_{11}^m + fc_{11}^p)(c_{11}^m + fc_{22}^p) - (c_{12}^m + fc_{21}^p)(c_{12}^m + fc_{12}^p)}; \quad (30)$$

$$O = \frac{c_{19}^p(c_{11}^m + fc_{22}^p) - c_{29}^p(c_{12}^m + fc_{12}^p)}{(c_{11}^m + fc_{11}^p)(c_{11}^m + fc_{22}^p) - (c_{12}^m + fc_{21}^p)(c_{12}^m + fc_{12}^p)}; \quad (31)$$

where $f = (1-\mu)/\mu$ is a middle parameter. The c_{11}^p, c_{12}^p, c_{13}^p, c_{21}^p, c_{22}^p and c_{23}^p are the electro-elastic constant components of the piezoelectric phase.

The density, longitudinal wave velocity and electromechanical conversion coefficient of a dense oblique 1-3 composite are respectively:

$$\rho_{(obl1-3)} = \rho_m(1-\mu) + \rho_p\mu; \quad (32)$$

$$c_{(obl1-3)} = \sqrt{\frac{c_{33(obl1-3)}^D}{\rho_{(obl1-3)}}}; \quad (33)$$

$$n_{(obl1-3)} = \frac{e_{(obl1-3)}S}{l_{(obl1-3)}}. \quad (34)$$

2.5. Finite Element Models of Sparse 1-3, Sparse Oblique 1-3 and Sparse Oblique 2-1-3 Composites

When the piezoelectric composite does not meet the conditions that vertical strains in two phases are the same and shear strains in two phases are the same, as shown in Eqs. (22) and (23), it is called a sparse piezoelectric composite. Three kinds of sparse composites, including sparse 1-3 composite, sparse oblique 1-3 composite, and sparse oblique 2-1-3 composite, are studied in this paper. Their electro-elastic constants cannot be calculated by theoretical analytical formulas. Instead, the finite element numerical calculation is used to complete the accurate calculation of the electro-elastic constants. The finite element simulation software ANSYS is used to model these three composites and calculate their elastic constant component c_{33}^D and piezoelectric constant component e_{33}. The specific operation processes include: pre-processing, geometric modeling, meshing, loading of boundary conditions and loads, solving, and post-processing.

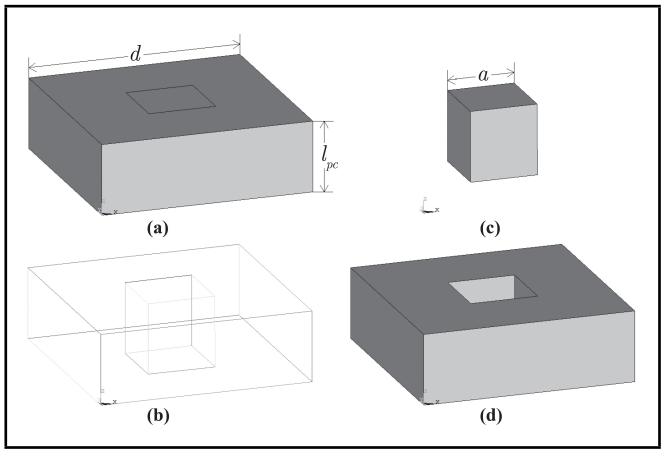

Figure 2. Unit cell of a sparse 1-3 composite. (a) complete body; (b) perspective view; (c) piezoelectric phase; (d) matrix phase.

2.5.1. Pre-processing

For sparse 1-3 composite, the element types of both piezoelectric phase and matrix phase are Solid5. For sparse oblique 1-3 and a sparse oblique 2-1-3 composites, the element types of both phases are Solid98. The material property part is needed to input the elastic constant matrix $[c^E]$, dielectric constant matrix $[\epsilon^S]$ and piezoelectric constant matrix $[e]$ of the piezoelectric phase, and the elastic constant matrix $[c^m]$ and dielectric constant matrix $[\epsilon^m]$ of the matrix phase. The material parameters of the piezoelectric phase and matrix phase are listed in Table 1.

2.5.2. Geometric modeling of sparse 1-3 composite

Since the structure of the piezoelectric composite is periodic, the properties of the whole composite can be characterized by a single unit cell containing the microstructure characteristics. The unit cell of sparse 1-3 composite is shown in Fig. 2.

In Fig. 2, l_{pc} is the thickness of the composite. The cross section of the unit cell is a square and d is the side length of the square, which is also the lateral distribution period of the piezoelectric rods. The cross section of the piezoelectric rod is also a square, and a is the side length of the square. The ratio of d and l_{pc} is called the aspect ratio:

$$\alpha = \frac{d}{l_{pc}}. \quad (35)$$

The volume fraction of the piezoelectric phase in a sparse 1-3 composite is:

$$\mu_{(sparse1-3)} = \frac{a^2}{d^2}. \quad (36)$$

2.5.3. Geometric modeling of sparse oblique 1-3 composite

The unit cell of a sparse oblique 1-3 composite is shown in Fig. 3. It is assumed that there is only one oblique piezoelectric rod within a unit cell.

In Fig. 3, l_{pc} is the thickness of the composite. The cross section of the unit cell is rectangular. d_1 is the length of the

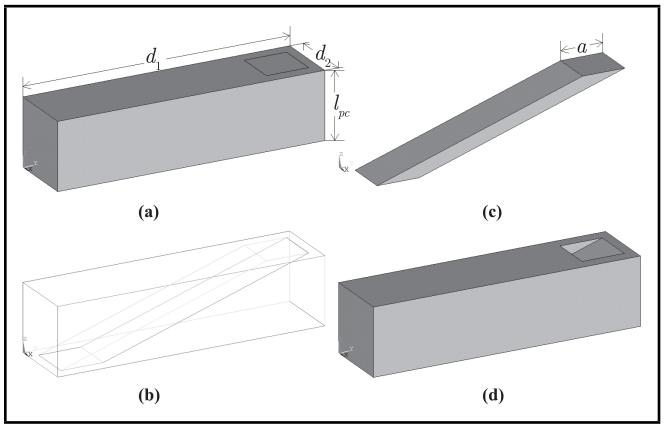

Figure 3. Unit cell of sparse oblique 1-3 composite. (a) complete body; (b) perspective view; (c) piezoelectric phase; (d) matrix phase.

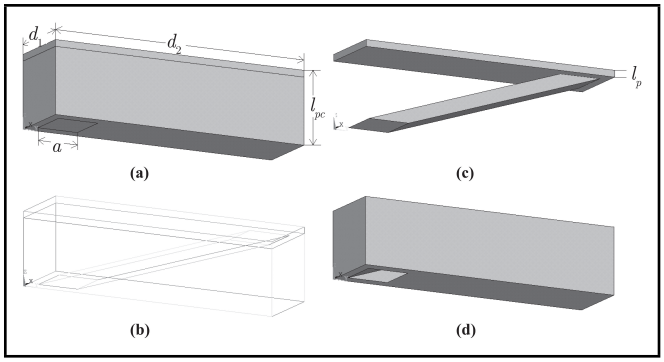

Figure 4. Unit cell of a sparse oblique 2-1-3 composite. (a) complete body; (b) perspective view; (c) piezoelectric phase; (d) matrix phase.

rectangular and is also the distribution period of the piezoelectric rods in the y-axis direction. d_2 is the width of the rectangular and is also the distribution period of the piezoelectric rods in the x-axis direction. The cross section of the piezoelectric rod is a square, and *a* is the side length of the square. The ratio of d_1 and l_{pc} is the aspect ratio in the y-axis direction, and the ratio of d_2 and l_{pc} is the aspect ratio in the x-axis direction:

$$\alpha_y = \frac{d_1}{l_{pc}}; \tag{37}$$

$$\alpha_x = \frac{d_2}{l_{pc}}. \tag{38}$$

The volume fraction of the piezoelectric phase in a sparse oblique 1-3 composite is:

$$\mu_{(sparse\_obl1-3)} = \frac{a^2}{d_1 d_2}. \tag{39}$$

2.5.4. Geometric modeling of sparse oblique 2-1-3 composite

The unit cell of a sparse oblique 2-1-3 composite is shown in Fig. 4. The composite is composed of a thin piezoelectric phase layer and a sparse oblique 1-3 composite layer.

In Fig. 4, l_{pc} is the thickness of a sparse oblique 2-1-3 composite. The cross section of the unit cell is a rectangular. d_1 and d_2 are the length and width of the rectangular, respectively. The cross section of the piezoelectric rod is a square, and a is the side length of the square. The aspect ratio in the y-axis direction is $\alpha_y = d_1/l_{pc}$, and the aspect ratio in the x-axis direction is $\alpha_x = d_2/l_{pc}$. l_p is the thickness of the thin piezoelectric phase layer. The ratio of l_p and l_{pc} is defined as β:

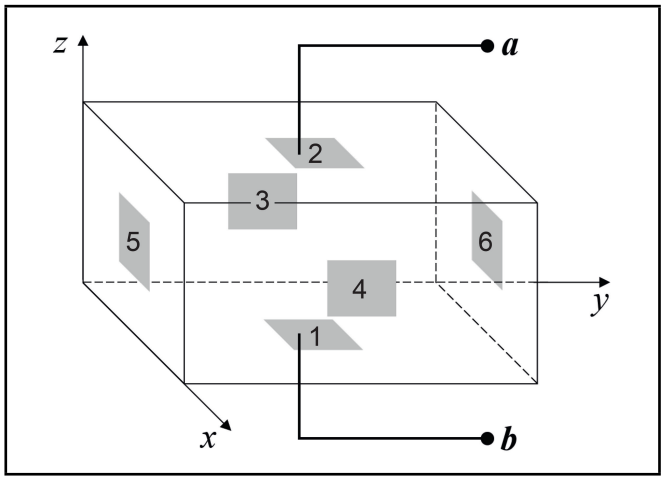

Figure 5. Illustration of boundary conditions and loads.

$$\beta = \frac{l_p}{l_{pc}}. \tag{40}$$

The volume fraction of the piezoelectric phase in a sparse oblique 2-1-3 composite is:

$$\mu_{(sparse\_obl2-1-3)} = \frac{a^2}{d_1 d_2}(1-\beta) + \beta. \tag{41}$$

2.5.5. Meshing

For a sparse 1-3 composite, the element types of both phases are Solid5, which is a coupled field 6-node hexahedral element. The mapped meshing method is used to partition the unit cell of the composite into a large number of hexahedral grid units. For a sparse oblique 1-3 and a sparse oblique 2-1-3 composites, the element types of both phases are Solid98, which is a coupled field 10-node tetrahedral element. The free meshing method is used to partition the unit cell into a large number of tetrahedral grid units. The degree of freedom option KEYOPT(1) is set as 3, and the degrees of freedom are UX, UY, UZ, and VOLT.

2.5.6. Loading of boundary conditions and loads

The constant electric displacement elastic constant component is (c_{33}^D), which represents the change of stress tensor component T_z caused by one unit change of strain tensor component S_z under the condition of constant electric displacement. (c_{33}^D) is defined as:

$$c_{33}^D = \left(\frac{\partial T_z}{\partial S_z}\right)_D = \left(\frac{\Delta T_z}{\Delta S_z}\right)\Big|_{D=0}; \tag{42}$$

where, the left side is the theoretical analytical definition, and the right side is the numerical calculation definition. The subscript D represents the constant electric displacement condition.

The piezoelectric (stress) constant component is e_{33}, which represents the increase of electric displacement tensor component D_z caused by one unit change of strain tensor component

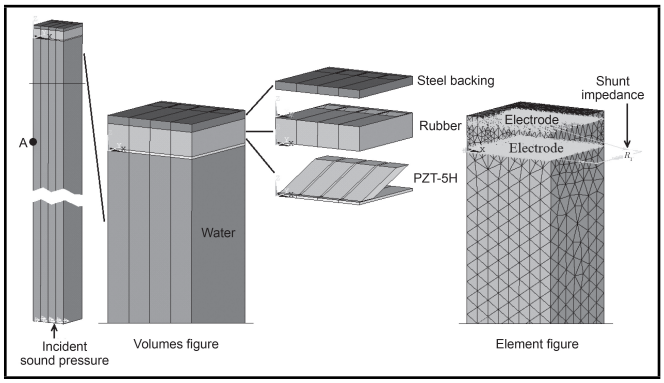

Figure 6. FE experimental measurement system of sound absorption coefficient.

S_z under the condition of constant electric field. e_{33} is defined as:

$$e_{33} = \left(\frac{\partial D_z}{\partial S_z}\right)_E = \left(\frac{\Delta D_z}{\Delta S_z}\right)\Big|_{E=0}; \tag{43}$$

where the subscript E represents the constant electric field condition. Fig. 5 is the unit cell of the composite, which is used to illustrate the boundary conditions and loads to be applied. For the calculation of both (c_{33}^D) and e_{33}, it is required to induce a change of strain tensor component S_z. To induce the change of S_z, Plane 1 should be fixed in z direction, and a pressure should be applied on Plane 2. To ensure that the strain tensor components in other directions are zero, Planes 3–6 should be fixed in their normal directions. The constant electric displacement condition is that electrodes A and B are open circuits. The constant electric field condition is that electrodes A and B are short circuits.

2.5.7. Solving and post-processing

In the solution part, the static analysis is conducted. In the post-processing part, the volume $(V_1, V_2, \ldots, V_n)$, strain component $(S_{z1}, S_{z2}, \ldots, S_{zn})$, stress component $(T_{z1}, T_{z2}, \ldots, T_{zn})$ and electric displacement component $(D_{z1}, D_{z2}, \ldots, D_{zn})$ values of all the grid units are picked up first. n represents the number of grid units. Then, the volumetrically-weighted averages of the strain component, stress component and electric displacement component values, namely $(\bar{S}_z)$, $(\bar{T}_z)$ and $(\bar{D}_z)$, are calculated. (c_{33}^D) and e_{33} can be obtained by the following two expressions:

$$c_{33(FEM)}^D = \frac{\overline{T}_z}{\overline{S}_z} = \frac{\sum_{j=1}^n T_{zj} V_j}{\sum_{j=1}^n S_{zj} V_j}; \tag{44}$$

$$e_{33(FEM)} = \frac{\overline{D}_z}{\overline{S}_z} = \frac{\sum_{j=1}^n D_{zj} V_j}{\sum_{j=1}^n S_{zj} V_j}. \tag{45}$$

3. MATERIAL PARAMETERS

The thickness of the composite is 3 cm, the thickness of the steel backing is 1 cm, and the surface area of both the composite and the steel backing is 0.3 m ×0.3 m. The material types and parameters of the piezoelectric phase and matrix phase are listed in Table 1. The material parameters and dimensions of steel, air and water are listed in Table 2.

Table 1. Material parameters of piezoelectric phase and matrix phase

Parameters	Piezoelectric Phase	Matrix Phase
	PZT-5H[24]	Rubber[10]
Density (kg/m^3)	7500	941.4
Longitudinal wave velocity (m/s)	4575.3	541.46
Young's modulus (Pa)	–	1.61×10^7
Poisson's ratio	–	0.49
Mechanical loss factor	1/65	0.212
Elastic constant c_{11} (Pa)	12.6×10^{10}	2.76×10^8
Elastic constant c_{12} (Pa)	7.95×10^{10}	2.65×10^8
Elastic constant c_{13} (Pa)	8.41×10^{10}	2.65×10^8
Elastic constant c_{33} (Pa)	11.7×10^{10}	2.76×10^8
Elastic constant c_{44} (Pa)	2.3×10^{10}	5.41×10^8
Elastic constant c_{66} (Pa)	2.35×10^{10}	5.41×10^8
Piezoelectric constant e_{15}(C/m^2)	17.0	–
Piezoelectric constant e_{31}(C/m^2)	-6.5	–
Piezoelectric constant e_{33}(C/m^2)	23.3	–
Relative dielectric constant ϵ_{11}/ϵ_0	1700	2.3
Relative dielectric constant ϵ_{33}/ϵ_0	1470	2.3

Table 2. Material parameters and dimensions of steel, water and air.

Parameters	Steel	Water	Air
Density (kg/m^3)	7840	1000	1.4
Longitudinal wave velocity (m/s)	5935	1483	340
Young's modulus (Pa)	21.6×10^{10}	–	–
Poisson's ratio	0.28	–	–
Thickness (mm)	10	semi-infinite	semi-infinite

3.1. FE Experimental Measurement of Sound Absorption Coefficient

In this study, a finite element (FE) simulation experiment based on the pipe pulse method[25] is used to measure the sound absorption coefficient of a sparse oblique 2-1-3 composite, so as to verify the theoretical calculation results of the sound absorption coefficient. The experimental measurement system, as shown in Fig. 6, consists of five parts: steel backing, rubber, piezoelectric ceramic, near-field water and shunt resistance. The piezoelectric composite layer is composed of four composite unit cells with a thickness of 3 cm. The cross section of the sound tube is a square with a side length of 12 cm, and the four side faces of the sound tube are fixed in their normal direction to simulate a square wave guide tube with a rigid boundary. The cross-sectional area of the composite is different in the experimental measurement system and the theoretical model, so the shunt resistance value used in the experiment needs to be converted from the shunt resistance value used in the theoretical model.

In the pipe pulse method, a plane sound wave is emitted into the water at one end of the sound tube. After a period of propagation, the incident sound wave reaches the composite layer and part of it is reflected back into the water. As long as the amplitudes of the incident sound wave and the reflection sound wave are measured, the sound absorption coefficient can be calculated. According to the rectangular wave guide tube theory, if only plane waves are transmitted inside the sound tube, the frequency of the incident sound wave must be less than the cut-off frequency 6.18 kHz. So the frequency range of the sound absorption coefficient measurement is set as 500–

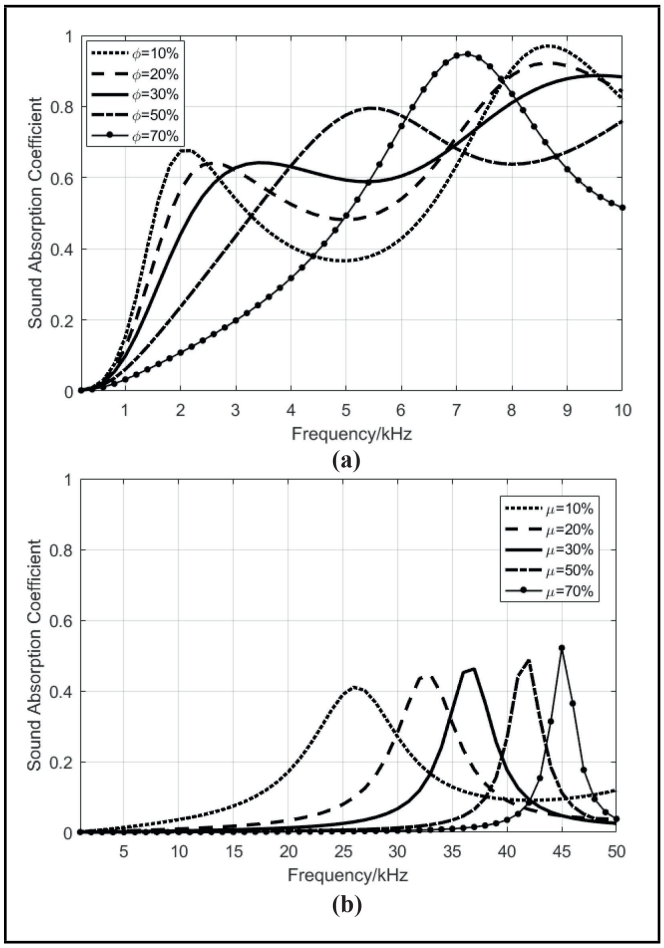

Figure 7. Open-circuit sound absorption coefficient of composites with different volume fractions of piezoelectric phase. (a) 0-3 composite; (b) 1-3 composite.

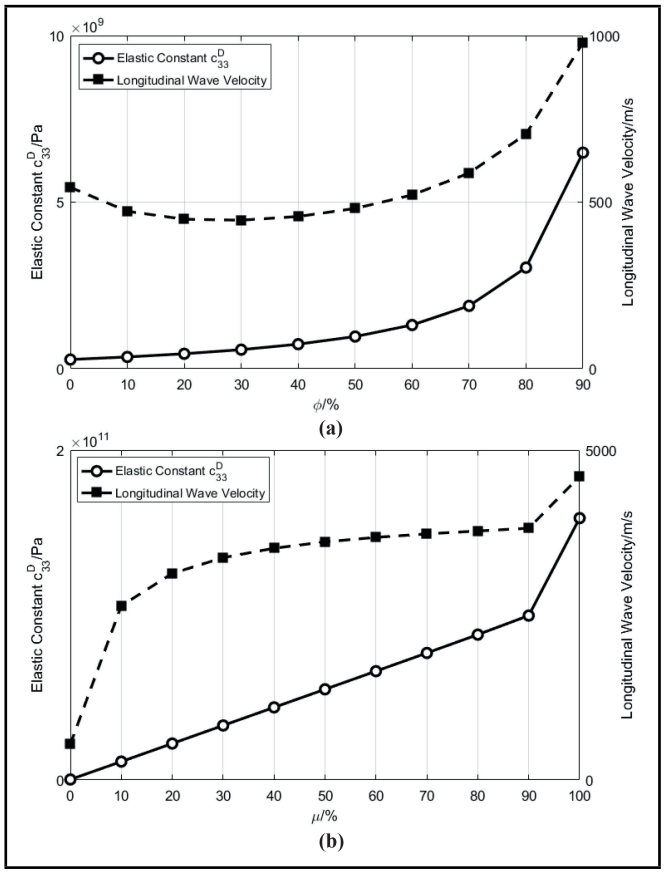

Figure 8. Elastic constant component and longitudinal wave velocity. (a) 0-3 composite; (b) 1-3 composite.

5000 Hz, and the frequency step length is 500 Hz. The incident sound pressure signal of a certain frequency is designed to be a sinusoidal wave with 10–30 cycles. A suitable point A is selected on the wall of the sound tube to extract the sound pressure signal, so that the incident signal and the reflection signal can be separated. The reflection sound pressure amplitude is $P_{ar}(f)$ and the incident sound pressure amplitude is $P_{ai}(f)$, then the sound absorption coefficient is:

$$A(f) = 1 - \left| \frac{P_{ar}(f)}{P_{ai}(f)} \right|^2 . \tag{46}$$

For different frequencies, the parameter settings of incident sound pressure signal, near-field water and transient analysis are shown in Table 3.

4. RESULTS AND DISCUSSION

4.1. Sound Absorption Performance of 0-3 and 1-3 Composites

The sound absorption coefficients of 0-3 composite with different volume fractions of piezoelectric phase ϕ are shown in Fig. 7(a). It can be seen that when increases from 10% to 70%, the frequency of the first peak of the sound absorption coefficient (hereinafter referred to as the first peak frequency) increases gradually from 2.2 kHz to 7.2 kHz. The first peak frequency mainly depends on the longitudinal wave velocity of the composite, which is determined by the elastic constant component c_{33} and density (see Eq. (13)). The influence of ϕ on the longitudinal wave velocity and c_{33} are shown in Fig. 8(a). It can be seen that the longitudinal wave velocity of a 0-3 composite is relatively low. When ϕ is between 10% and 70%, the longitudinal wave velocity is between 445.8 m/s and 587.1 m/s. The smaller c_{33} is, the smaller the first peak frequency is, which is good for improving the sound absorption coefficient within the low frequency band 1–3 kHz.

The sound absorption coefficients of 1-3 composite with different volume factions of piezoelectric phase μ are shown in Fig. 7(b). It can be seen that when μ increases from 10% to 70%, the first peak frequency increases gradually from 26 kHz to 45 kHz, which is obviously higher than that of the 0-3 composite. The main reason is that the longitudinal wave velocity and c_{33} of the 1-3 composite are relatively high, as shown in Fig. 8(b). When μ is between 10% and 70%, the longitudinal wave velocity is between 2640 m/s and 3730 m/s, which is obviously higher than that of the 0-3 composite. Obviously, high first peak frequency caused by high longitudinal wave velocity is not good for improving the sound absorption coefficient within the low frequency band 1–3 kHz.

The sound absorption mechanism in Fig. 7 is the mechanical damping of the piezoelectric composite. In order to realize semi-active sound absorption and effectively adjust the sound absorption coefficient within the low frequency band, it is necessary to connect the shunt circuit to the composite. The appropriate shunt circuit type depends on the type of the piezo-

Table 3. Parameter settings of FE experimental measurement of sound absorption coefficient

Parameters of Incident Sinusoidal Signal				Parameters of Near-field Water		Parameters of Transient Analysis	
Frequency/Hz	Cycle Number	Time/ms	Length/m	Length/m	Grid Number	Time/ms	Substep Number
500	10	20.0000	29.6600	40	300	55	2750
1000	10	10.0000	14.8300	20	300	35	3500
1500	15	10.0000	14.8300	20	400	35	4375
2000	20	10.0000	14.8300	20	600	35	7000
2500	20	8.0000	11.8640	20	700	35	8750
3000	20	6.6667	9.8867	10	400	15	5000
3500	20	5.7143	8.4743	10	500	15	5000
4000	20	5.0000	7.4150	10	600	15	6000
4500	30	6.6667	9.8867	10	700	15	7500
5000	30	6.0000	8.8980	10	800	15	7500

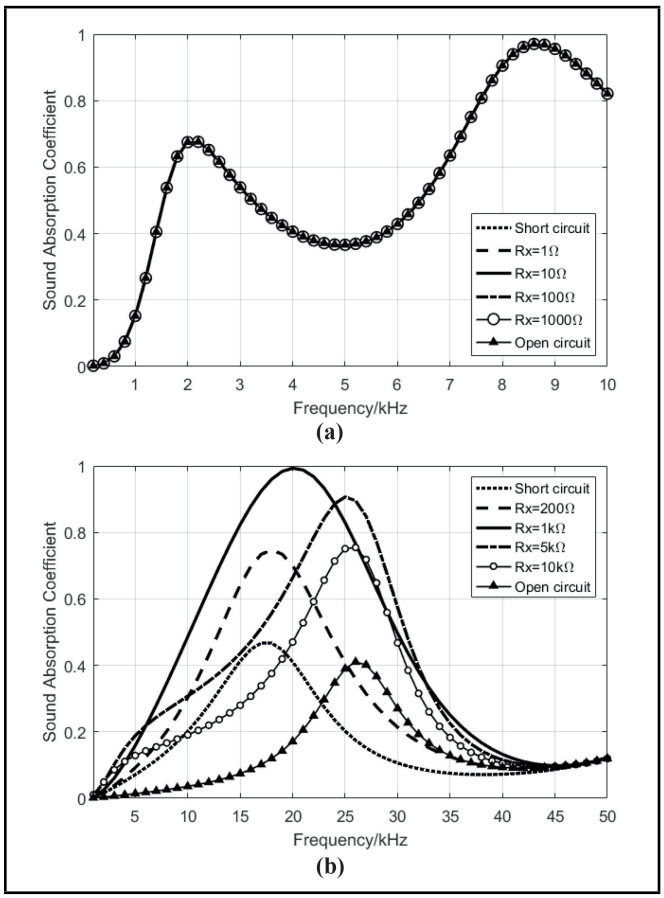

Figure 9. Sound absorption coefficient of composites with different shunt resistances. (a) 0-3 composite ($\phi = 10\%$); (b) 1-3 composite ($\mu = 10\%$).

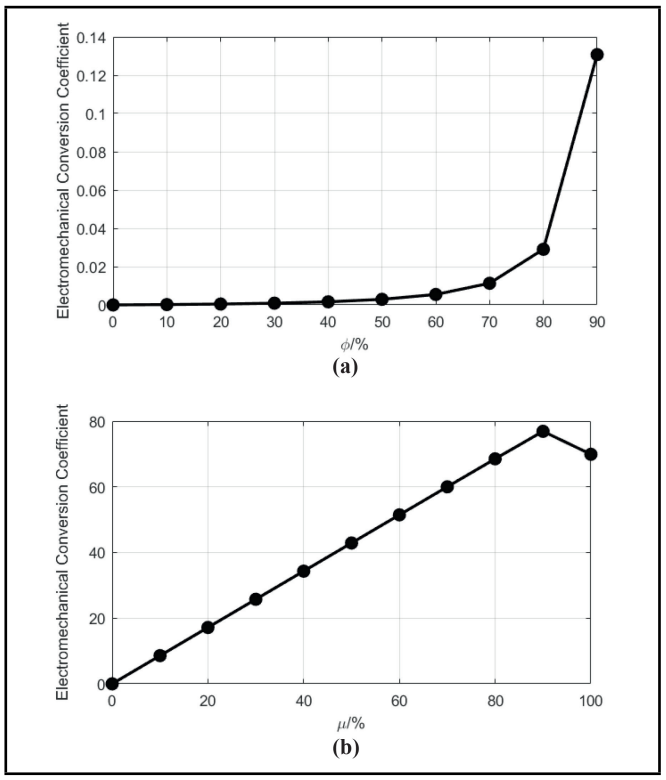

Figure 10. Electromechanical conversion coefficient. (a) 0-3 composite; (b) 1-3 composite.

electric composite. The appropriate type for the 0-3 composite is resistance and negative capacitance series circuit,[10] and the appropriate type for the 1-3 composite is negative resistance and capacitance or inductance series circuit.[12] The realization of negative capacitance and negative resistance requires active components such as operational amplifiers and the stability and accuracy of the shunt circuit are difficult to guarantee. In contrast, the shunt circuit composed of passive components such as resistance, capacitance and inductance is easier to implement and is more stable. Since the shunt resistance is the only component that can dissipate energy in semi-active sound absorption, this paper aids in designing the structure of resistance shunt type piezoelectric composite.

The sound absorption coefficients of 0-3 composite ($\phi = 10\%$) with different shunt resistances R_x are shown in Fig. 9(a). It can be seen that the sound absorption coefficient has no obvious change under the conditions of short circuit, connected with different shunt resistances and open circuit. This happens because the electromechanical conversion coefficient of the 0-3 composite is very small, as shown in Fig. 10(a), and the value does not exceed 0.13. It can be analyzed from the electromechanical equivalent circuit in Fig. 1(b) that the influence degree of the shunt impedance Z_x on the physical properties of the composite depends on the transformer parameter in the equivalent circuit n, which is the electromechanical conversion coefficient. Since the electromechanical conversion coefficient of the 0-3 composite is very small, the shunt resistance has almost no influence on the physical properties of the composite, and therefore the sound absorption coefficient has almost no change.

The sound absorption coefficients of 1-3 composite ($\mu = 10\%$) with different shunt resistances R_x are shown in Fig. 9(b). It can be seen that the sound absorption coefficient has an obvious change under the conditions of short circuit,

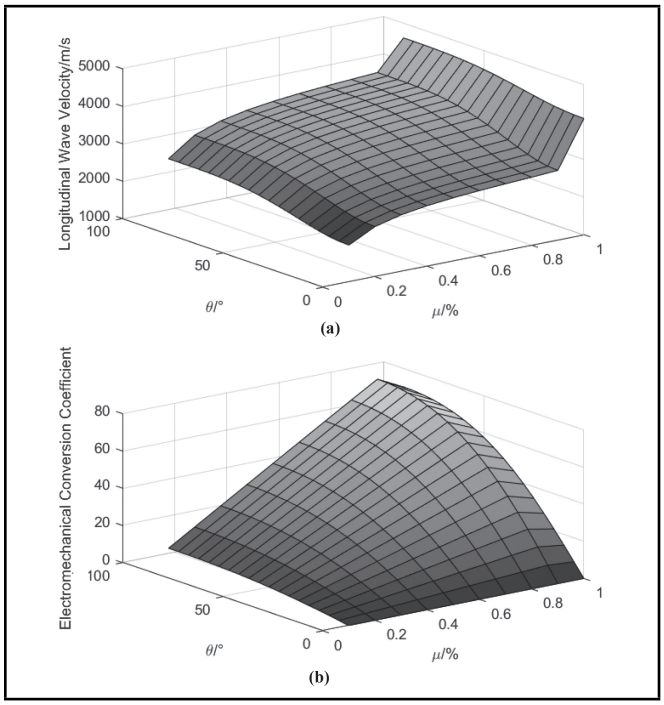

Figure 11. Property parameters of a dense oblique 1-3 composite. (a) longitudinal wave velocity; (b) electromechanical conversion coefficient.

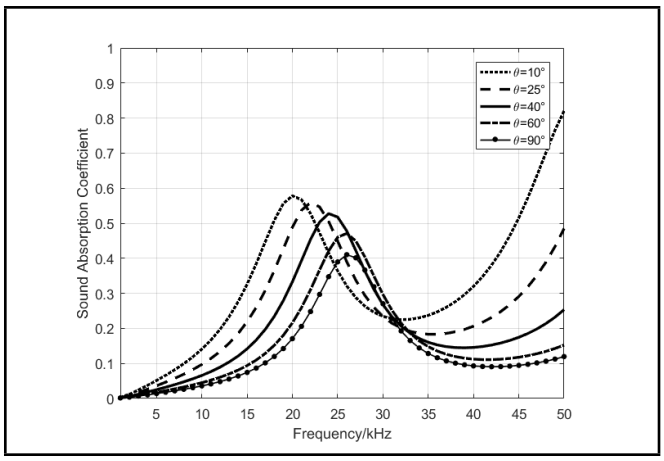

Figure 12. Open-circuit sound absorption coefficient of a dense oblique 1-3 composite ($\mu = 10\%$) with different inclination angles.

connected with different shunt resistances and an open circuit. This is because the electromechanical conversion coefficient of 1-3 composite is much higher than that of the 0-3 composite, as shown in Fig. 10(b). When $\mu = 10\%$, the electromechanical conversion coefficient $n = 8.581$. The high electromechanical conversion coefficient is good for effectively adjusting the physical properties of the composite by connecting the shunt resistance and, therefore, effectively adjusting the sound absorption coefficient and realizing semi-active sound absorption.

Through the above calculation and analysis, it can be concluded that:

(1) Low longitudinal wave velocity is good for reducing the first peak frequency and improving the sound absorption coefficient within low frequency band.

(2) A high electromechanical conversion coefficient is good for effectively adjusting the sound absorption coefficient by connecting shunt resistance.

(3) If we want to improve the sound absorption coefficient within low frequency band by connecting shunt resistance, low longitudinal wave velocity and high electromechanical conversion coefficient are the physical properties that the piezoelectric composite should have.

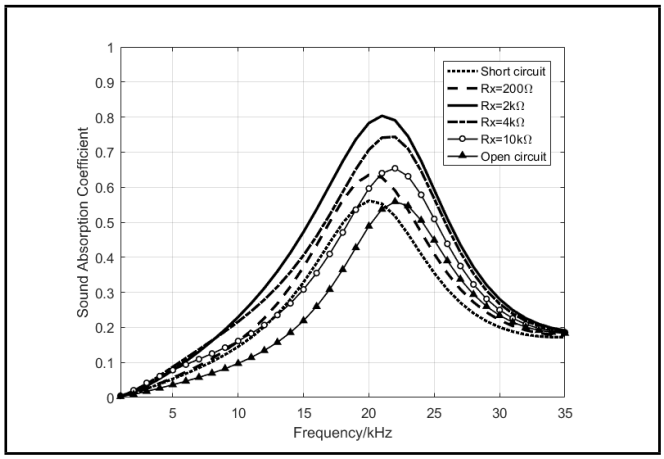

Figure 13. Sound absorption coefficient of a dense oblique 1-3 composite ($\mu = 10\%$,$\theta = 25°$) with different shunt resistances.

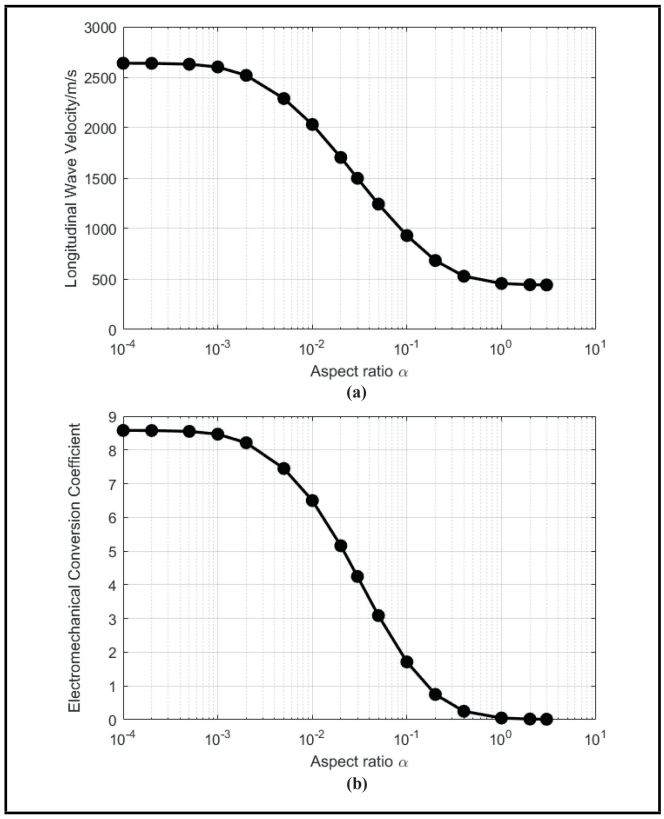

Figure 14. Property parameters of a sparse 1-3 composite with different aspect ratio α. (a) longitudinal wave velocity; (b) electromechanical conversion coefficient.

The longitudinal wave velocity of the 0-3 composite is low (445.8 m/s when $\phi = 10\%$), but its electromechanical conversion coefficient is also low (0.0002 when $\phi = 10\%$). The electromechanical conversion coefficient of the 1-3 composite is high (8.58 when $\mu = 10\%$), but its longitudinal wave veloc-

Table 4. Comparison of property parameters of 6 types of piezoelectric composites.

Composite type	Volume fraction of piezoelectric phase	Inclination angle	Aspect ratio	Longitudinal wave velocity (m/s)	Electromechanical conversion coefficient
0-3	10%	–	–	445.8	0.0002
Sparse oblique 1-3	20%	27°	y:4, x:1	402.6	0.0282
		90°	y:4, x:1	397.7	0.0633
Sparse 1-3	10%	–	3	441.1	0.0135
		–	2	443.4	0.0192
		–	1	455.6	0.0503
Sparse oblique 2-1-3	28%	18°	y:4,x:1	404.9	0.6258
		21°	y:4,x:1	417.9	0.9993
		24°	y:4,x:1	447.9	1.4980
		27°	y:4,x:1	501.7	2.1390
Dense oblique 1-3	10%	10°	–	2035.0	1.7990
		25°	–	2232.0	4.2230
		40°	–	2440.0	6.1170
Dense 1-3	10%	–	–	2640.0	8.5810

ity is also high (2640 m/s when $\mu = 10\%$). Therefore, both of them are obviously not the suitable piezoelectric composite type used for resistance shunt underwater semi-active sound absorption.

The longitudinal wave velocity and electromechanical conversion coefficient of the composite are determined by the property and connectivity of the two phases. Under the same density and same dimension condition, the longitudinal wave velocity of the composite depends on the elastic constant component c_{33}, and the electromechanical conversion coefficient depends on the piezoelectric constant component e_{33}. In the 0-3 composite, the matrix phase is connected in three directions, so the longitudinal wave velocity of the composite mainly depends on the longitudinal wave velocity of the matrix phase. Since the material of the matrix phase is soft, c_{33} is small, conclusively, the longitudinal wave velocity of the composite is low. The piezoelectricity of the composite is determined by the connectivity of the piezoelectric phase. The piezoelectric particles of the 0-3 composite are dispersed in the matrix phase and are disconnected in three directions, so the piezoelectricity of the composite is weak, namely, e_{33} is small, and therefore the electromechanical conversion coefficient is low. In the 1-3 composite, the piezoelectric rods are vertically embedded in the matrix phase and are connected in the thickness direction, so the piezoelectric phase has a greater influence on the longitudinal wave velocity of the composite. Since the material of the piezoelectric phase is hard, c_{33} is large and therefore the longitudinal wave velocity of the composite is high. The connectivity of the piezoelectric rods in the thickness direction makes the piezoelectricity of the composite high, namely $e_{33}$is large, and therefore the electromechanical conversion coefficient is high.

4.2. Sound Absorption Performance of a Dense Oblique 1-3 Composite

The calculation results of the longitudinal wave velocity and electromechanical conversion coefficient of a dense oblique 1-3 composite are shown in Figs. 11(a) and 11(b). The two coordinate axes on the horizontal plane of the 3D figure are the volume fraction of the piezoelectric phase μ and the inclination angle θ, respectively. It can be seen from the figure that for a certain μ, with the decrease of θ, the longitudinal wave velocity decreases gradually, and the electromechanical conversion coefficient also decreases gradually.

In the actual preparation process, in order to ensure the mechanical strength of a dense oblique 1-3 composite, the volume fraction of piezoelectric phase μ should not be too low, and the piezoelectric rods should not be too thin or too oblique. Hence μ is set as not less than 10%, and θ is set as not less than 10°. When $\mu = 10\%$ and θ decreases from 90° to 10°, the longitudinal wave velocity decreases from 2640 m/s to 2035 m/s, and the electromechanical conversion coefficient decreases from 8.581 to 1.799. When $\theta = 90°$, a dense oblique 1-3 composite is just a dense 1-3 composite. It can be seen that when μ is the same, the longitudinal wave velocity of a dense oblique 1-3 composite is lower than that of a dense 1-3 composite, and the electromechanical conversion coefficient is smaller than that of a dense 1-3 composite. Compared with that of the 0-3 composite, the longitudinal wave velocity of a dense oblique 1-3 composite is higher, and the electromechanical conversion coefficient is larger.

The first peak frequency of the sound absorption coefficient will decrease with the decrease of the longitudinal wave velocity. Figure 12 shows the sound absorption coefficient of a dense oblique 1-3 composite with different inclination angles when μ is 10%. The curve of $\theta = 90°$ in the figure is exactly the same as the curve of $\mu = 10\%$ in Fig. 7(b). It can be seen that when θ decreases from 90° to 10°, the first peak frequency gradually decreases from 26 kHz to 20 kHz, which is significantly lower than that of the 1-3 composite but significantly higher than that of the 0-3 composite shown in Fig. 7(a).

Although the electromechanical conversion coefficient of a dense oblique 1-3 composite is smaller than that of the 1-3 composite, it is much larger than that of the 0-3 composite. An electromechanical conversion coefficient of not less than 1.799 is sufficient for the shunt resistance to cause an obvious change in the sound absorption coefficient. Figure 13 shows the sound absorption coefficient of a dense oblique 1-3 composite ($\mu = 10\%, \theta = 25°$) with different shunt resistance R_x. It can be seen that the first peak value, first peak frequency and bandwidth of the sound absorption coefficient have obvious changes under the conditions of short circuit, connected

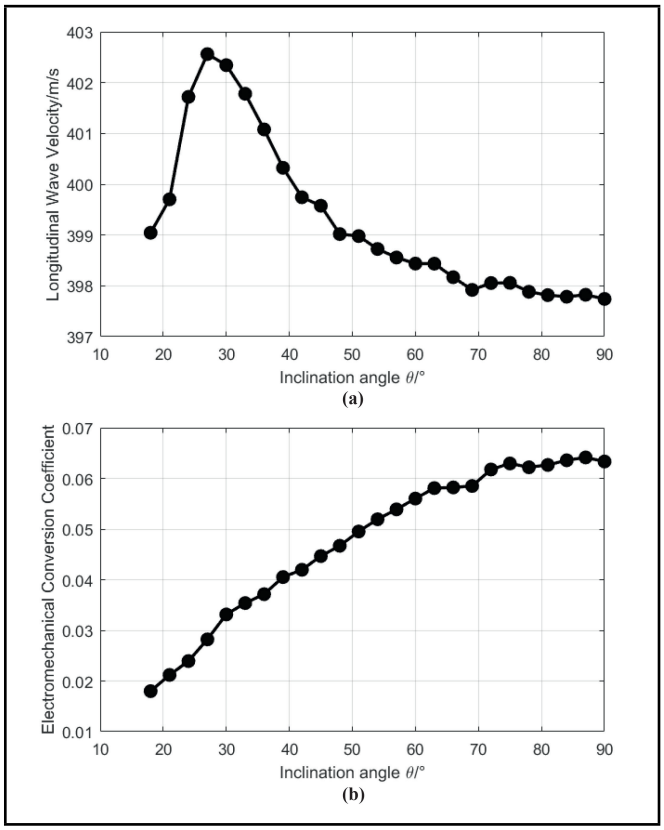

Figure 15. Property parameters of a sparse oblique 1-3 composite with different inclination angle θ. (a) longitudinal wave velocity; (b) electromechanical conversion coefficient.

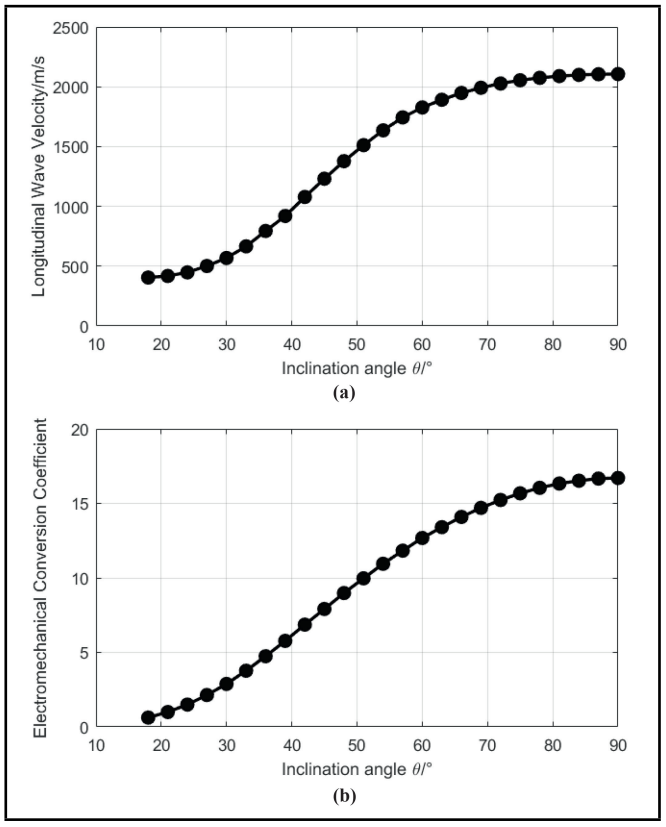

Figure 16. Property parameters of a sparse oblique 2-1-3 composite with different inclination angle θ. (a) longitudinal wave velocity; (b) electromechanical conversion coefficient.

with different shunt resistances and open circuit.

In conclusion, compared with a dense 1-3 composite, a dense oblique 1-3 composite can reduce the longitudinal wave velocity to a certain extent without reducing the electromechanical conversion coefficient too low, but still cannot reduce the longitudinal wave velocity to that of the 0-3 composite, as shown in Table 4. Therefore, a dense oblique 1-3 composite is also not the suitable piezoelectric composite type used for resistance shunt underwater semi-active sound absorption.

4.3. Sound Absorption Performance of Sparse 1-3 Composite

Both the 1-3 composite and the oblique 1-3 composite studied above are dense composites, in which the lateral spatial scale of the piezoelectric rods is very fine, and the composite can be regarded as an effective homogeneous media. When pressure is applied on the surface of a dense composite, the piezoelectric phase and the matrix phase will produce the same vertical strain. In a piezoelectric composite, the elastic constant component c_{33} of the piezoelectric phase is much larger than that of the matrix phase (see Table 1), that is, the piezoelectric phase is harder than the matrix phase. If the vertical strains of the two phases are the same, the composite will be hard, namely the elastic constant component c_{33} is large, and therefore the longitudinal wave velocity will be large (see Eqs. (20) and (33)).

In order to reduce the longitudinal wave velocity of the 1-3 composite and the oblique 1-3 composite, the lateral spatial scale of the piezoelectric rods can be increased, namely the piezoelectric rods are sparsely distributed in the matrix phase. This composite is called a sparse piezoelectric composite. When pressure is applied on the surface of a sparse composite, the vertical strains produced by the two phases are different. The softer matrix phase will produce larger vertical strain than the harder piezoelectric phase does, so the composite will become softer, the elastic constant component c_{33} will become smaller, and therefore longitudinal wave velocity will decrease.

The volume fraction of piezoelectric phase is set as 10%, and the aspect ratio α changes from 10^{-4} to 3. Eqs. (44) and (45) are used to calculate the elastic constant component $c^D_{33(sparse1-3)}$ and piezoelectric constant component $c_{33(sparse1-3)}$ and Eqs. (19), (20) and (21) are used to calculate the density, longitudinal wave velocity and electromechanical conversion coefficient of the composite. The variations of the longitudinal wave velocity and electromechanical conversion coefficient of a sparse 1-3 composite with different aspect ratio α are shown in Figs. 14(a) and 14(b). As can be seen from the figures, when $\alpha = 10^{-4}$, the composite is just a dense composite. Its longitudinal wave velocity is equal to the longitudinal wave velocity ($\mu = 10\%$) in Fig. 8(b) and and its electromechanical conversion coefficient is equal to the electromechanical conversion coefficient ($\mu = 10\%$) in Fig. (10)(b). When α increases gradually, the longitudinal wave velocity decreases gradually. When $\alpha = 3$, the longitudinal wave velocity decreases to 441.1 m/s. The longitudinal wave velocity of a sparse 1-3 composite is much lower than that of a dense 1-3 composite, while the electromechanical conversion coefficient of a sparse 1-3 composite is also much smaller than that of a

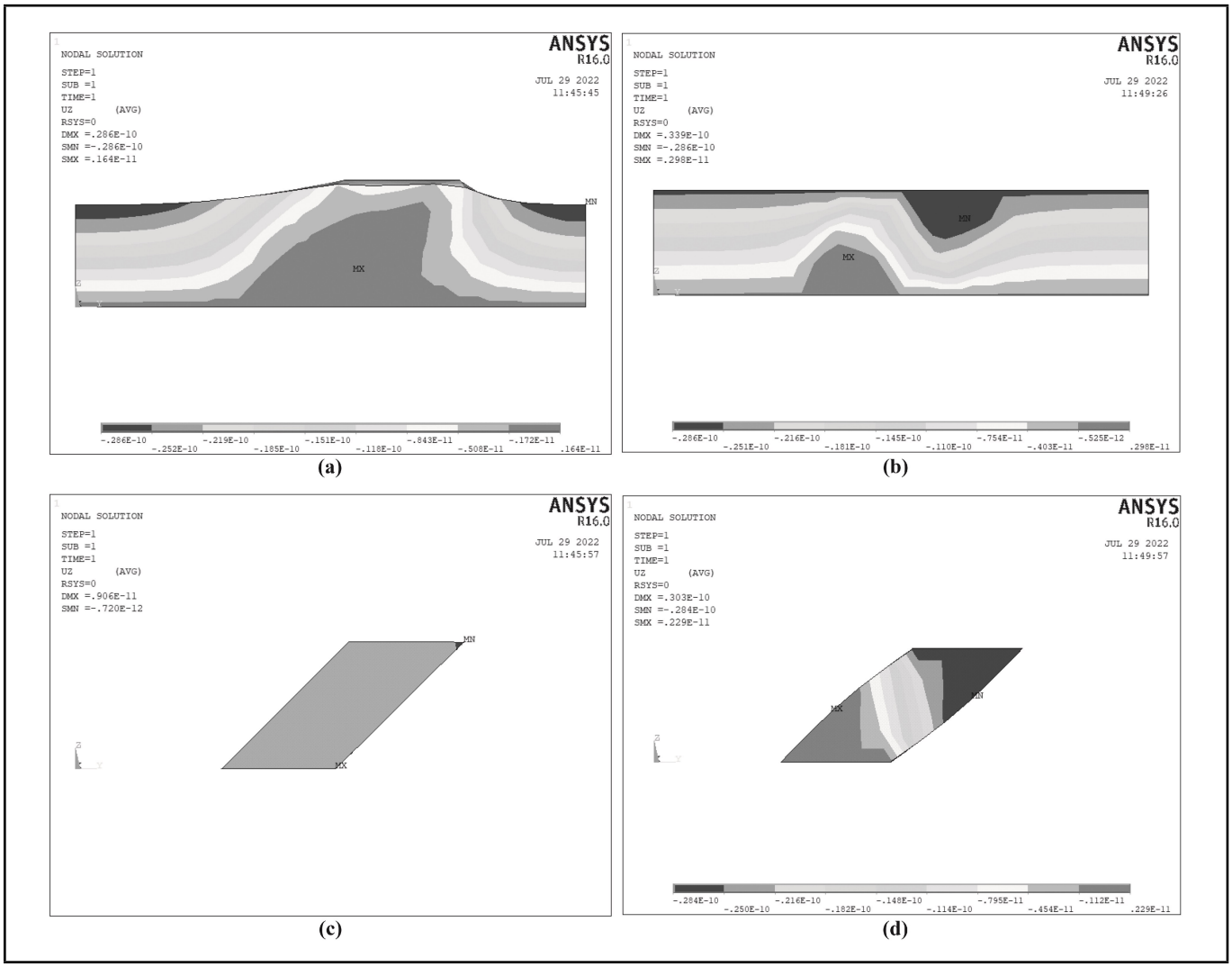

Figure 17. Comparison of z-direction displacement of two composites. (a) matrix phase of a sparse oblique 1-3 composite; (b) matrix phase of a sparse oblique 2-1-3 composite; (c) piezoelectric rod of a sparse oblique 1-3 composite; (d) piezoelectric rod of a sparse oblique 2-1-3 composite.

dense 1-3 composite. When $\alpha = 3$, the electromechanical conversion factor reduces to 0.0135. The property parameter data of a sparse 1-3 composite are added to Table 4.

4.4. Sound Absorption Performance of Sparse Oblique 1-3 Composite

In order to ensure the mechanical strength of the composite and at the same time reduce the longitudinal wave velocity as much as possible, the volume fraction of the piezoelectric phase is set as 20%, the aspect ratio in the y-axis direction $\alpha_y = 4$, the aspect ratio in the x-axis direction $\alpha_x = 1$, and the inclination angle changes from 18° to 90°. Equations (44) and (45) are used to calculate the elastic constant component $c^D_{33(sparse\_obl1-3)}$ and piezoelectric constant component $e_{33(sparse\_obl1-3)}$ and Eqs. (32), (33) and (35) are used to calculate the density, longitudinal wave velocity and electromechanical conversion coefficient of the composite. The variations of the longitudinal wave velocity and electromechanical conversion coefficient of a sparse oblique 1-3 composite with different inclination angles θ are shown in Fig. 15(a) and 15(b). As shown in the figures, when θ gradually increases, the longitudinal wave velocity of the composite first increases and then decreases. When $\theta = 27°$, the longitudinal wave velocity reaches the maximum value 402.6 m/s. When θ gradually increases, the electromechanical conversion coefficient of the composite increases gradually, and the maximum is 0.0633. It can be seen that, similar to the case of a sparse 1-3 composite, although the longitudinal wave velocity of a sparse oblique 1-3 composite is much lower than that of a dense oblique 1-3 composite, the electromechanical conversion coefficient of a sparse oblique 1-3 composite is also much smaller.

The property parameter data of a sparse oblique 1-3 composite are added to Table 4. The data in the table show that the longitudinal wave velocity of a sparse composite is much lower than that of a dense composite, which is close to that of 0-3 composite. However, the electromechanical conversion coefficient decreases by about two orders of magnitude. Although it is much higher than that of a 0-3 composite, it is not enough to change the sound absorption coefficient of the composite by connecting shunt resistance. Therefore, both a sparse 1-3 composite and a sparse oblique 1-3 composite are also not the suitable resistance shunt type piezoelectric composite. How to reduce the longitudinal wave velocity and, at the same time, maintain a relatively large electromechanical conversion factor is the next step to explore.

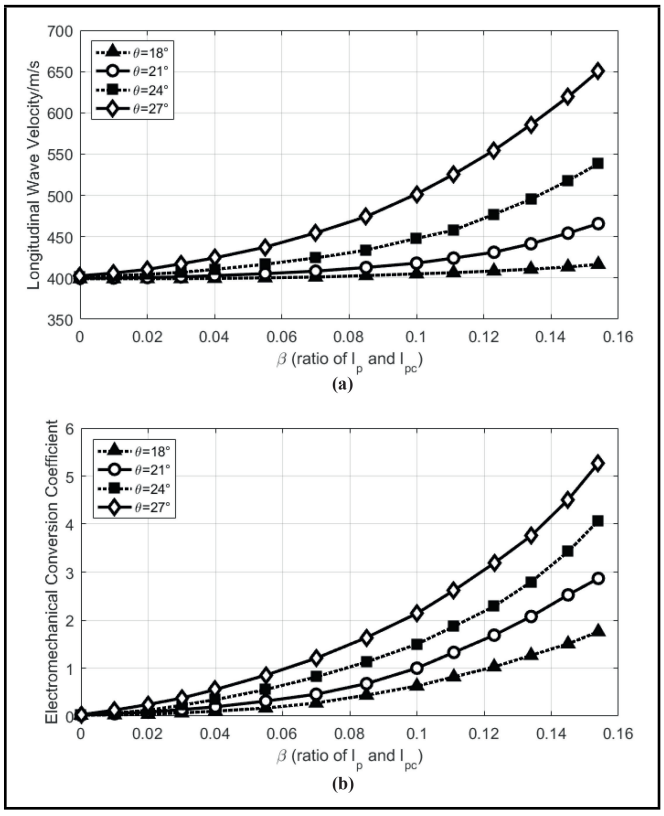

Figure 18. Property parameters of a sparse oblique 2-1-3 composite with different ratio β. (a) longitudinal wave velocity; (b) electromechanical conversion coefficient.

4.5. Sound Absorption Performance of a Sparse Oblique 2-1-3 Composite

Due to the sparse distribution of the piezoelectric rods, when pressure is applied on the surface of a sparse 1-3 composite or a sparse oblique 1-3 composite, the matrix phase will produce a large vertical displacement while the piezoelectric phase will produce a small vertical displacement. Under the same dimension condition, the electromechanical conversion coefficient of the composite depends on the magnitude of its piezoelectric constant component e_{33}, namely the strength of piezoelectricity. If the piezoelectric rods in the composite can not produce a large enough vertical displacement, then the piezoelectricity of the composite will be weak and the electromechanical conversion coefficient will be low. In order to improve the piezoelectricity of the composite, it is necessary to effectively transfer the pressure applied on the surface of the composite to the piezoelectric rods, so that the piezoelectric rods can produce a larger vertical displacement. Therefore we propose to add a thin piezoelectric phase layer on the surface of the sparse oblique 1-3 composite. In this thin layer, the piezoelectric phase is connected in two directions, so this composite can be called a sparse oblique 2-1-3 piezoelectric composite.

In order to ensure the mechanical strength of the composite and at the same time reduce the longitudinal wave velocity as much as possible, the volume fraction of the piezoelectric phase is set as 28% (the volume fraction of piezoelectric phase in a sparse oblique 1-3 composite is 20%), the aspect ratio in the y-axis direction $\alpha_y = 4$, the aspect ratio in the x-axis direction $\alpha_x = 1$, the ratio $\beta = 0.1$ and the inclination angle changes from 18° to 90°. The variations of the longitudinal wave velocity and electromechanical conversion coefficient of a sparse oblique 2-1-3 composite with different inclination angle θ are shown in Figs. 16(a) and 16(b). As shown in the figures, when θ gradually decreases, the longitudinal wave velocity of the composite decreases gradually, and the electromechanical conversion coefficient also decreases gradually.

The property parameter data of a sparse oblique 2-1-3 composite are added to Table 4. As can be seen from the table, compared with a sparse oblique 1-3 composite, the longitudinal wave velocity of a sparse oblique 2-1-3 composite increases a little, still close to that of 0-3 composite, and much lower than that of the dense oblique 1-3 composite. Compared with a sparse oblique 1-3 composite, the electromechanical conversion coefficient of a sparse oblique 2-1-3 composite increases greatly, which can reach the same order of magnitude as that of the dense oblique 1-3 composite.

From a sparse oblique 1-3 composite to a sparse oblique 2-1-3 composite, the reason why the piezoelectricity can be improved is that the pressure applied on the surface of the composite can be effectively transferred to the piezoelectric rods by the thin piezoelectric phase layer, so that the piezoelectric rods can produce a larger vertical displacement. The piezoelectricity of the piezoelectric composite depends on the electromechanical conversion coefficient n. Under the same dimension condition, n depends on the piezoelectric constant component e_{33} (see Eqs. 21 and (24)). e_{33} is the increase of electric displacement tensor component D_z caused by one unit change of strain tensor component S_z (see Eq. (43)). In the composite, the piezoelectric phase has piezoelectricity, while the matrix phase has no piezoelectricity. When the sound pressure acts on the surface of a sparse oblique 1-3 composite, the vertical displacement generated by the top of the piezoelectric rod is small, then the change of strain tensor component S_z is small, the increase of electrical displacement tensor component D_z is small, therefore e_{33} of the composite is small and the piezoelectricity is weak. When the sound pressure acts on the surface of a sparse oblique 2-1-3 composite, the presence of the thin piezoelectric phase layer makes the top of the piezoelectric rod produce a larger vertical displacement, then the change of S_z becomes larger, the increase of D_z becomes larger, therefore e_{33} of the composite is large and the piezoelectricity is strong. Figure 17 shows the z-direction displacement of the two composites. It can be seen that the matrix phases of both composites have a large vertical displacement (the maximum absolute value is 0.286×10^{-10} m), while the vertical displacement of the piezoelectric rods has a large difference. The vertical displacement of the piezoelectric rod of a sparse oblique 1-3 composite is very small (0.720×10^{-12} m), while the vertical displacement of the piezoelectric rod of a sparse oblique 2-1-3 composite is large (the maximum absolute value is 0.284×10^{-10} m), which is close to the vertical displacement of the matrix phase.

The thickness of the thin piezoelectric phase layer will affect the longitudinal wave velocity and piezoelectricity of a sparse oblique 2-1-3 composite. Let the thickness of the composite l_{pc} be 3 cm and remain unchanged. As shown in Eq. (36), β is the ratio of the thickness of the thin piezoelectric phase

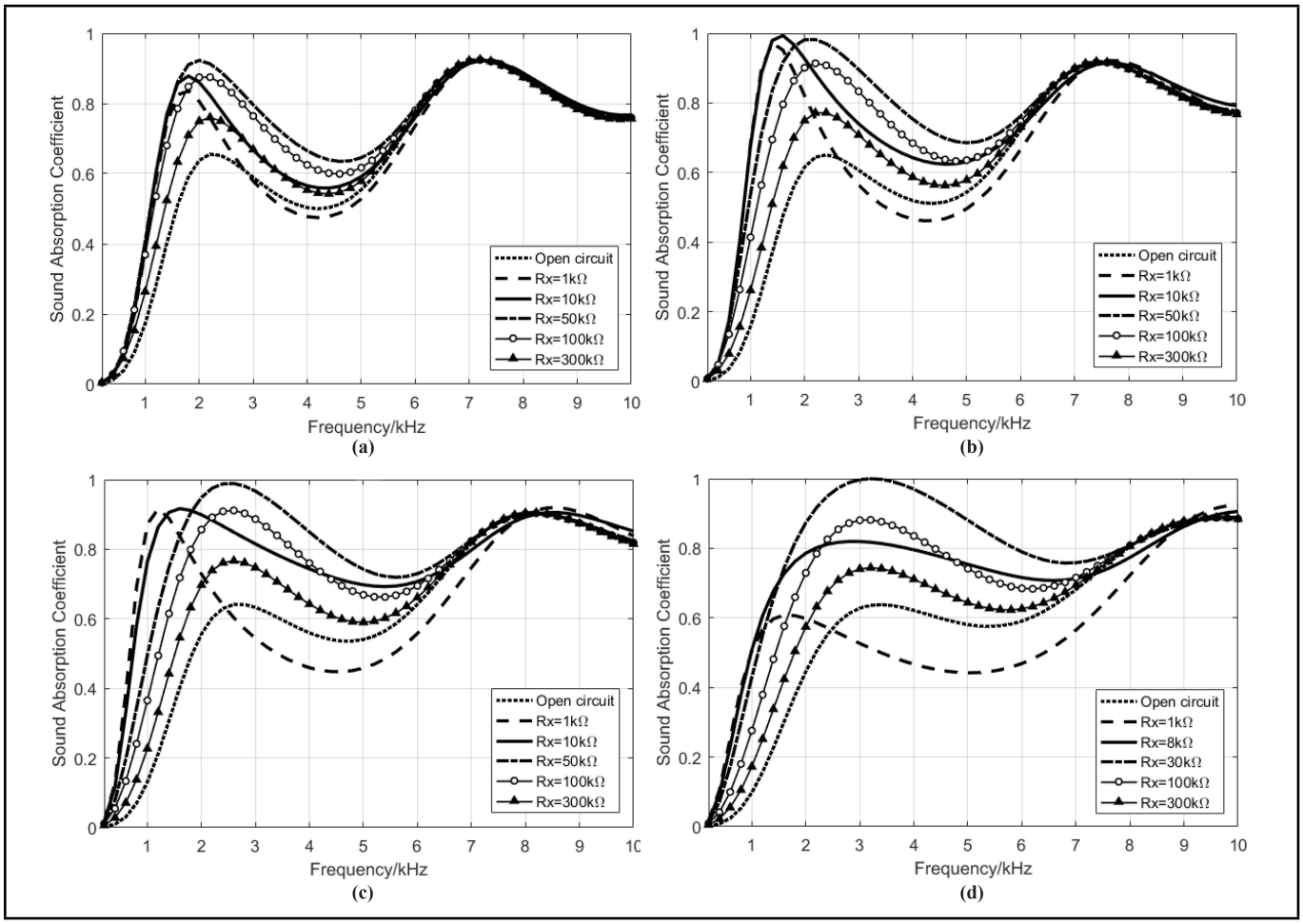

Figure 19. Sound absorption coefficient of a sparse oblique 2-1-3 composite with different shunt resistances. (a) inclination angle $\theta = 18°$; (b) inclination angle $\theta = 21°$; (c) inclination angle $\theta = 24°$; (d) inclination angle $\theta = 27°$.

layer l_p and the thickness of the composite l_{pc}. The increase of β represents the increase of l_p. Let the volume fraction of piezoelectric phase in a sparse oblique 1-3 composite be 20% and remain unchanged. According to Eq. (37), when β increases, the volume fraction of the piezoelectric phase in a sparse oblique 2-1-3 composite will increase. When the inclination angle θ is respectively set as 18°, 21°, 24° and 27° and the ratio β varies from 0 to 0.154, the variations of the longitudinal wave velocity and electromechanical conversion coefficient of a sparse oblique 2-1-3 composite are shown in Figs. 18(a) and 18(b). As shown in the figures, when β gradually increases, namley the thickness of the thin piezoelectric phase layer l_p increases, both the longitudinal wave velocity and electromechanical conversion coefficient increase gradually, and the piezoelectricity is enhanced. $\beta = 0.1$ in Fig. 18 corresponds to the parameter setting of β in Fig. 16. At this point, the longitudinal wave velocity is still relatively small, which is conducive to improving the low-frequency sound absorption coefficient, and the electromechanical conversion coefficient has been increased to the level that the shunt resistance can effectively adjust the sound absorption coefficient. So, in the following calculation of sound absorption coefficient, the ratio β is set as 0.1.

When the inclination angle θ is set as 18°, 21°, 24° and 27° respectively, the sound absorption coefficients of a sparse oblique 2-1-3 composite with different shunt resistance R_x are shown in Figs. 19(a), 19(b), 19(c) and 19(d). It can be seen that when the composite is open circuit, for the four different inclination angles, the first peak frequencies of the sound absorption coefficient are all relatively low, which are 2.2 kHz, 2.4 kHz, 2.6 kHz and 3.4 kHz, respectively, and the sound absorption coefficients within the low frequency band 1–3 kHz are relatively large. When the composite is connected with different shunt resistances, for the four different inclination angles, the first peak value, first peak frequency and bandwidth of the sound absorption coefficient all have obvious changes. The larger the inclination angle is, the more obvious the change is. In the following two cases, the sound absorption coefficient within the low frequency band 1–3 kHz can be significantly improved by connecting shunt resistance:

1. When the inclination angle θ is 21° and the shunt resistance is 10 kΩ, the sound absorption coefficient within the low frequency band 1–3 kHz is above 0.6779, and the largest value is 0.9935.

2. When the inclination angle θ is 24° and the shunt resistance is 10 kΩ, the sound absorption coefficient within the low frequency band 1–3 kHz is above 0.7642, and the largest value is 0.9168.

When a sparse oblique 2-1-3 composite is under the following four conditions: (1) inclination angle $\theta = 21°$ and

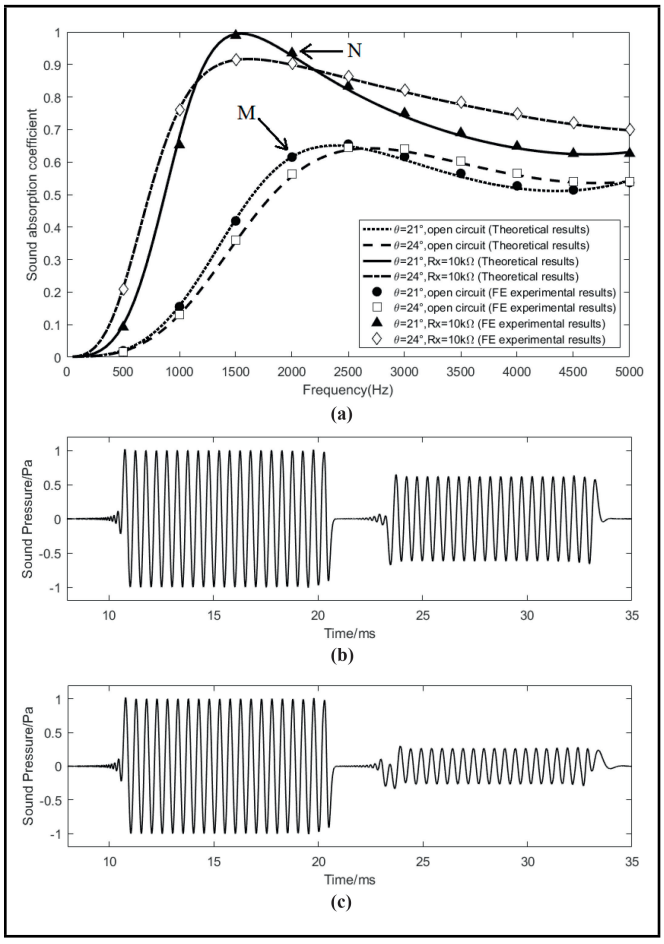

Figure 20. (a) Theoretical calculation results and FE experimental measurement results of sound absorption coefficient of a sparse oblique 2-1-3 composite; (b) 2 kHz sound pressure signal detected in the pipe pulse method experiment (inclination angle $\theta = 21^\circ$ and open circuit); (c) 2 kHz sound pressure signal detected in the pipe pulse method experiment (inclination angle $\theta = 21^\circ$ and shunt resistance $R_x = 10$ kΩ.

open circuit, (2) inclination angle $\theta = 21^\circ$ and shunt resistance $R_x = 10$ kΩ, (3) inclination angle $\theta = 24^\circ$ and open circuit, (4) inclination angle $\theta = 24^\circ$ and shunt resistance $R_x = 10$ kΩ, the theoretical calculation results and FE experimental measurement results of sound absorption coefficient are shown in Fig. 20(a). Two points M and N in Fig. 20(a) are taken as examples and Figs. 20(b) and 20(c) show the 2 kHz sound pressure signals detected in the experimental measurement of sound absorption coefficient using the pipe pulse method when a sparse oblique 2-1-3 composite is under the above conditions (1) and (2), respectively. The left side is the incident signal and the right side is the reflection signal. By extracting the amplitudes of the incident signal and the reflection signal, the sound absorption coefficients of M and N points in Fig. 20(a) can be calculated. As can be seen from Fig. 20(a), for a certain condition, the experimental measurement results of sound absorption coefficient are nearly consistent with the theoretical calculation results, therefore the theoretical calculation results have been verified to be correct.

In conclusion, a sparse oblique 2-1-3 composite can reduce the longitudinal wave velocity and, at the same time, maintain a relatively large electromechanical conversion coefficient, and therefore can improve the sound absorption coefficient within the low frequency band, 1–3 kHz, by connecting the shunt resistance. Hence it is a suitable resistance shunt type piezoelectric composite for underwater semi-active sound absorption.

5. CONCLUSIONS

In this paper, a kind of resistance shunt type piezoelectric composite used in underwater semi-active sound absorption was designed, and its sound absorption performance was analyzed. The structure design process of the composite is summarized as follows:

1. Firstly, the influence of the property parameters of the 0-3 composite and a dense 1-3 composite used in the existing research work on the sound absorption coefficient was studied. The conclusion is that if we want to improve the sound absorption coefficient within the low frequency band by connecting the shunt resistance, the composite should have low longitudinal wave velocity and a high electromechanical conversion coefficient.

2. Then, according to the design objective of the physical properties, the structure of the piezoelectric composite is gradually modified. The longitudinal wave velocity, electromechanical conversion coefficient and sound absorption performance of a dense oblique 1-3 composite, a sparse 1-3 composite, a sparse oblique 1-3 composite and a sparse oblique 2-1-3 composite were studied.

3. Finally, it was confirmed that a sparse oblique 2-1-3 composite is a suitable piezoelectric composite type for resistor shunt underwater semi-active sound absorption. The reason is that the oblique and the sparse distribution of the piezoelectric rods can effectively reduce the longitudinal wave velocity of the composite, and the thin piezoelectric phase layer can ensure that the composite has a large electromechanical conversion coefficient.

ACKNOWLEDGEMENTS

This work was supported by Natural Science Foundation of Beijing (6222038).

AUTHORS' CONTRIBUTIONS

All authors contributed to the study conception and design. Material preparation, data collection and analysis were performed by Yang Sun and Bo Hua. The first draft of the manuscript was written by Yang Sun and all authors commented on previous versions of the manuscript. All authors read and approved the final manuscript.

REFERENCES

[1] Fu, Y. F., Kabir, I. I., Yeoh, G. H.,and Peng, Z. X. A Review on polymer-based materials for underwater sound absorption, *Polymer Testing*, **96**, 107115-1-20, (2021). https://doi.org/10.1016/j.polymertesting.2021.107115

[2] Bai, H. B., Zhan, Z. Q, Liu, J. C, and Ren, Z. Y. From local structure to overall performance, *Materials*, **12**(16), 2509-1-17, (2019). https://doi.org/10.3390/ma12162509

[3] Zhao, D., Zhao, H. G., Yang, H. B., and Wen, J. H. Optimization and mechanism of acoustic absorption of Alberich coatings on a steel plate in water, *Applied Acoustics*, **140**, 183–187, (2018). https://doi.org/10.1016/j.apacoust.2018.05.027

[4] Luo, Y. Q., Lou, J. J., Zhang, Y. B., and Li, J. R. Sound-absorption mechanism of structures with periodic cavities, *Acoustics Australia*, **49**(2), 371-383, (2021). https://doi.org/10.1007/s40857-021-00233-6

[5] Ayub, M., Fouladi, M. H., Ghassem, M., Nor, M. J. M., Najafabadi, H. S., Amin, N.,and Zulkifli, R. Analysis on multiple perforated plate sound absorber made of coir fiber, *International Journal of Acoustics and Vibration*, **19**(3), 203–211, (2014). https://doi.org/10.20855/ijav.2014.19.3354

[6] Yang, J., Zhao, X. Y., Wang, K. J., Song, H., and Cui, Z. X. Influence of deformation on sound-absorbing performance under hydrostatic pressure, *International Journal of Acoustics and Vibration*, **27**(4), 344–353, (2022). https://doi.org/10.20855/ijav.2022.27.41876

[7] Wang, W. J. and Thomas, P. J. Low-frequency active noise control of an underwater large-scale structure with distributed giant magnetostrictive actuators, *Sensors and Actuators A*, **263**, 113–121, (2017). https://doi.org/10.1016/j.sna.2017.05.044

[8] Pyun, J. Y., Park, B. H., Kim. Y. H., Won, Y. B., Yi, H., Lee, J. M., Seo, H. S., and Park, K. K. Design and analysis of an active reflection controller that reduce acoustic signal refer to the angle of incidence, *Sensors*, **21**(17), 5793-1-18, (2021). https://doi.org//10.3390/s21175793

[9] Zhang, J. M., Chang, W., Varadan, V. K., and Varadan, V. V. Passive underwater acoustic damping using shunted piezoelectric coatings, *Smart Materials and Structures*, **10**, 414–420, (2001). https://doi.org/10.1088/0964-1726/10/2/404

[10] Yu, L. G., Li, Z. H., and Ma, L. L. Theoretical analysis of underwater sound absorption of 0-3 type piezoelectric composite coatings, *Acta Physica Sinica*, **61**(2), 024301-1-8, (2012). https://doi.org/10.4028/10.7498/aps.61.024301

[11] Feng, L., Li, S. P., and Hu, Q. The research of damped absorbing layer based on piezoelectric shunt, *Proc. 2017 Symposium on Piezoelectricity, Acoustic Waves, and Device Applications*, Chengdu, China, (2017). https://doi.org/10.1109/SPAWDA.2017.8340332

[12] Sun, Y., Li, Z. H., Huang, A. G., and Li, Q. H. Semi-active control of piezoelectric coating's underwater sound absorption by combining design of the shunt impedances, *Journal of Sound and Vibration*, **355**, 19–38, (2015). https://doi.org/10.1016/j.jsv.2015.06.036

[13] Zhang, Z. F., Li, S. D., Wang, J. X., and Huang, Q. B. Low-frequency broadband absorption of semi-active composite anechoic coating with subwavelength piezoelectric arrays in hydrostatic environments, *Results in Physics*, **30**, 104879-1-17, (2021). https://doi.org/10.1016/j.rinp.2021.104879

[14] Wang, M. F., Yi, K. J., and Zhu, R. Tunable underwater low-frequency sound absorption via locally resonant piezoelectric metamaterials. *Journal of Sound and Vibration*, **548**, 117514-1-13, (2023).https://doi.org//10.1016/j.jsv.2022.117514

[15] Forward, R. L. Electronic damping of vibrations in optical structures, *Applied Optics*, **18**(5), 690–697, (1979). https://doi.org/10.1364/AO.18.000690

[16] Hagood, N. W. and Flotow, A. von. Damping of structural vibations with piezoelectric materials and passive electrical metworks, *Journal of Sound and Vibration*, **146**(2), 243—268, (1991). https://doi.org/10.1016/0022-460X(91)90762-9

[17] Guo, H., Zhang, Y. R., Yuan, T., Qian, P. S., Cheng, Q., and Wang, Y. S. Vibration attenuation optimization in a rod with different periodic piezoelectric shunting configurations, *International Journal of Acoustics and Vibration*, **26**(3), 212–220, (2021). https://doi.org/10.20855/ijav.2021.26.31751

[18] Liu, X., Wang, C. Q., Zhang, Y. M., and Huang, L. X. Investigation of broadband sound absorption of smart micro-perforated panel (MPP) absorber, *International Journal of Mechanical Sciences*, **199**, 106426-1-11, (2021). https://doi.org/10.1016/j.ijmecsci.2021.106426

[19] Kim. J. and Jung, Y. C. Broadband noise reduction of piezoelectric smart panel featuring negative-capacitive-converter shunt circuit, *Journal of the Acoustical Society of America*, **120**(4), 2017–2025, (2006). https://doi.org/10.1121/1.2259791

[20] Larbi, W., Deue, J. F., Ohayon, R., and Sampaio, R. Coupled FEM/BEM for control of noise radiation and sound transmission using piezoelectric shunt damping, *Applied Acoustics*, **86**, 146–153, (2014). https://doi.org/10.1016/j.apacoust.2014.02.003

[21] Furukawa, T., Ishida, K., and Fukada, E. Piezoelectric properties in the composite systems of polymers and pzt ceramics, *Journal of Applied Physics*, **50**(7), 4904–4912, (1979). https://doi.org/10.1063/1.325592

[22] Smith, W. A. and Auld, B. A. Modeling 1-3 composite piezoelectrics: thickness-mode oscillations, *IEEE Trans. Ultrason. Ferroelectr. Freq. Control*, **38**(1), 40–47, (1991). https://doi.org//10.1109/58.67833

[23] Baz, A. and Tempia, A. Active piezoelectric damping composites, *Sensors and Actuators A*, **112**, 340–350, (2004). https://doi.org/10.1016/j.sna.2004.01.021

[24] Wang, R. J. *Underwater Acoustic Materials Manual*, Science Press, Beijing, (1983).

[25] Wei, Z. Y., Hou, H., Gao, N. S., Huang, Y. K., and Yang, J. H. Measurement of sound absorption using a single fixed microphone in a circular pulse-tube, *Acta Acustica United with Acustica*, **105**(6), 1228–1236, (2019). https://doi.org/10.3813/AAA.919399